MSAS – Final project
GOCE

Adrian Burton Parisi - 940789 | 10710691
Gianluca Vighi - 953611 | 10501496
Viktor Schütz - 962153 | 10757226

1 The real system

On the 17th of March in 2009 a satellite with an overall mass of about 1050kg, developed by the European Space Agency and named ***Gravity field and steady-state Ocean Circulation Explorer* (GOCE)**, was launched into space from the Russian Kosmodrom Plessezk. The objective of this mission was to determine the geoids and gravitational anomalies of Earth with an accuracy of 1cm in geoid height, 10^{-6}g in acceleration, and a spatial resolution of 100 km or less over the surface of the Earth. To fulfil the mission goals GOCE was equipped with a *Gravity Gradiometer*, consisting of three pairs of electrostatic accelerometers, which were installed in three orthogonal directions to detect linear and angular accelerations. Two GPS receivers were used for precise orbit-determination, measuring the position and velocity, while a pair of star trackers determined the attitude of the spacecraft.[Can+09]

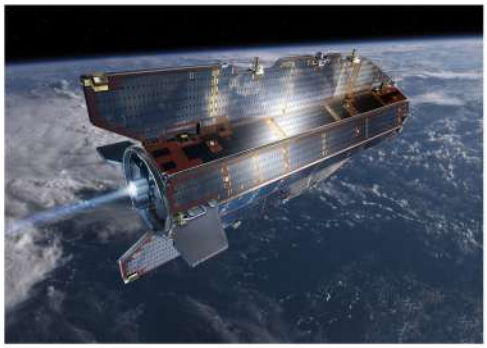

Figure 1: Artist impression of GOCE in space.[13]

GOCE maintained a sun-synchronous low earth orbit with an altitude between 240 and 270km, where the drag effects, caused by the thermosphere are still significant.[Mar+03] In order to minimise these drag effects the design resulted in a slim body with a length of 5.3m and a cross sectional area of 1.1m^2. It was symmetrical in the horizontal plane and equipped with two winglets that provided passive aerodynamic stability.

To achieve such precise measurements with the gravity gradiometer, all non-gravitational forces acting on GOCE had to be counteracted. Therefore, the ***Drag Free and Attitude Control System* - (DFAC)** was developed to accomplish this drag compensation. Two QinetiQ T5 Kaufman-type ion thrusters, each able to produce up to 20mN of thrust, were chosen for the main actuators for the DFAC and installed at the rear of GOCE.[Edw+] This system provided continuous drag compensation until an off-nominal condition occurred when the pressure in the tank fell below the minimum pressure required for the ion thrusters to work due to low propellant on the 18th October 2013. The mission ended on the 11th November of 2013 with reentry occurring, near the south coast of South-America.[Gin+14]

2 The physical model

The physical model will represent a simplified version of the DFAC used by GOCE consisting of a single electrostatic accelerometer, a solenoid valve to control propellant flow, and an ion thruster, in contrast to the three electrostatic accelerometer pairs and two ion thrusters that GOCE actually possessed. Furthermore, the assumption that the longitudinal axis of GOCE will always be in the direction of drag is imposed and is independent to the orbital velocity vector, which simplifies the model to a one dimensional problem. This assumption can be further justified on account of the existence of the passive stabilisation winglets which will naturally cause GOCE to orient to this direction. An orbital model was used to simulate the spacecraft within a low earth orbit with J_2 and drag perturbations affecting the orbital elements. Additional perturbations such as solar radiation pressure, the effect of gravitational forces caused by other celestial bodies, and further minuscule perturbations have been neglected.

2.1 Accelerometer

Applying the mechanical and electric domains the electrostatic accelerometer consists of a seismic mass, modelled as a point mass, that is free to move, but maintained at a reference position by two electrodes by applying electrostatic forces. The range of motion of the seismic-mass is parallel to the axis of the spacecraft and is taken as positive in the direction of GOCE. Collectively, the electrodes and the seismic mass can be modelled as two ideal capacitors connected in series. The associated *capacitor plate separation* is defined by the distance from the surface of the seismic mass to the electrode and the *capacitor area*, is the surface of the face of the seismic mass.

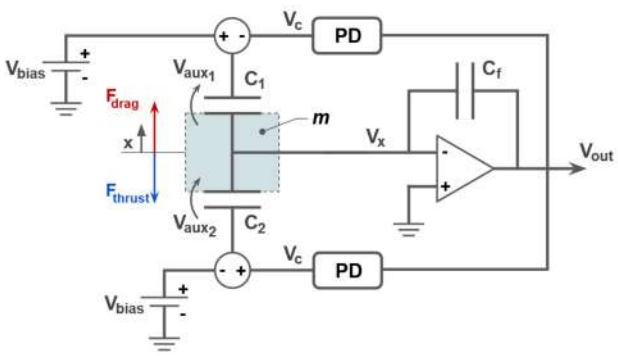

Figure 2: Physical model of the Accelerometer with the reference direction and apparent forces of drag and thrust shown in addition, to the circuitry. The real mass placement has been overlayed the ideal capacitors.

On account of the typical separation being on the order of 100 μm the electric field between the electrode and mass is assumed to be constant.[Tou+99] The drag acting on the spacecraft leads to a position-change of the seismic-mass relative to the reference point, resulting in an apparent force acting in the positive direction, as seen in Figure 2, with the opposite effect when considering the thrust. The movement of the mass modifies the capacitance of the ideal capacitors, which in turn alters the voltage across each capacitor. This voltage, deemed V_x, is fed into an ideal operational amplifier with the output voltage fed back through a PD controller before summing with a voltage bias and acting as a potential difference across the capacitors.

In addition, the parasitic resistance and inductance effects of the capacitor, and the parasitic oscillations of the amplifier are assumed to be small and are therefore, neglected. Furthermore, a resistor in parallel to the amplifier, which would aid in handling the saturation of the amplifier, has not been considered due to its component-dependency and thus being out of scope for the model.

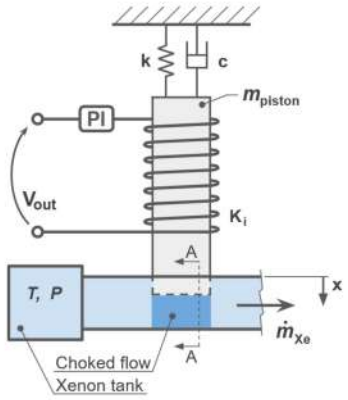

Figure 3: Physical model of the solenoid control valve with the PI controller affecting the current through the system. The null reference position is taken as fully open.

2.2 Solenoid Valve

The solenoid valve as a whole determines the amount of propellant entering the ion thruster and is modelled within the mechanical and fluid domain. It consists of a Xenon propellant tank, a pipe, an electric coil and a piston. The piston is modelled as a simple spring-dashpot system with an additional force generated by a coil surrounding it. The coil is modelled as an inductor with the voltage potential provided by the accelerometer. The position of the piston defines the opened area of the valve which in turns, under the assumption of choked flow, provides a mass flow of propellant to the ion thruster. The spring within the solenoid is considered ideal, and the friction of the piston and any viscous effects occurring during the motion of the piston are accumulated in the damping term. The force generated by the coil surrounding the piston is due to a magnetic field stored within the inductor. All non-linear and dissipative effects such as magnetic saturation and hystersis effects have been neglected and the physics of the solenoid is condensed into a single coefficient K_i, which is multiplied with the

current within the wire to obtain a force. The wire resistance has been disregarded, in addition to any parasitic capacitance within the coil. The temperature is also assumed to be constant to discount any effects on temperature dependent electrical properties. Furthermore, the working temperature and pressure within propellant tank is assumed to be constant and follows the ideal gas laws with isentropic flow conditions, to achieve choked flow within the valve-opening. The flow is considered steady and no pressure gradients are present within the pipes.

2.3 Ion Thruster

The ion thruster has been reduced to a one dimensional system. This is achieved by neglecting all dimensional effects, that are not on the axis in the direction of the beam. Furthermore, it is assumed that all of the Xenon gas atoms entering the thruster are singly ionised within the ionisation chamber and is equivalently neutralised at the exit of the thruster, neglecting any charge imbalances caused by electron build up within the system. The emission of neutralising electrons does not affect the overall thrust. Moreover, the accelerator grid does not experience any erosion and therefore is considered as ideal and consecutively accelerates all the ions to an identical speed, starting from an assumed null speed.

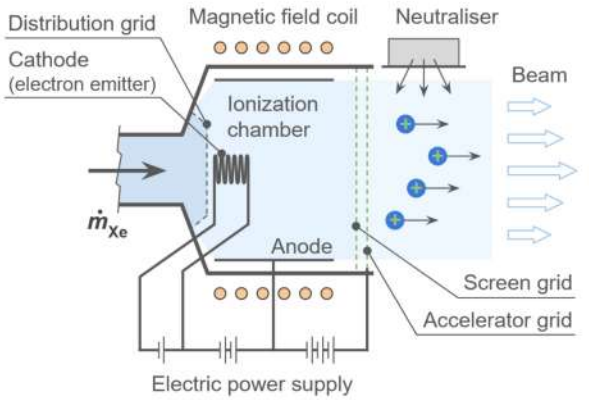

Figure 4: Physical model of the ion thruster. All components have been simplified down to an ionisation chamber which is assumed as ideal and the grids which accelerate the ions. All other components are not modelled.

3 The Mathematical Model

3.1 Accelerometer

The accelerometer states variables are the position and velocity of the seismic mass denoted x_a and v_a, respectively, and the voltage output of the accelerometer, V_{out}. The reference position and origin of the mass is taken to be the central point between the electrodes.

Modelling the mass-electrode systems as a capacitor, as mentioned in Section 2.1, with the definition of capacitance, $C = \varepsilon A/d$, where ε, A, and d, represent the permittivity, area of the capacitor plate, and gap between the mass surface and electrode, respectively. The voltage, V_x, shown within Figure 2 was computed by considering voltages across each ideal capacitor, C_1 and C_2, resulting in

$$V_x = \frac{V_b x_a}{g} \tag{1}$$

where V_b and g, are the voltage bias and the distance between the electrode and the reference position, respectively. Considering and applying the capacitor characteristic equation, $I = C\dot{V}$, to the parallel capacitor, C_f, and defining the voltage, V_f, across this capacitor is equal and opposite to V_{out} such that $V_{out} = -V_f$. The current going into C_f can be defined by the difference in capacitance between C_1 and C_2,

$$I_f = \frac{\partial\left(C_2 - C_1\right)}{\partial x} v_a V_b \tag{2}$$

Substituting these values and equations together results in the differential state equation for V_{out},

$$\dot{V}_{out} = \frac{2\varepsilon A}{C_f} \frac{g^2 + x_a^2}{\left(g^2 - x_a^2\right)^2} v_a V_b \tag{3}$$

A proportional-derivative controller was used in order to alter the voltages across each of the ideal capacitors. This controller took in an input of V_{out} and $\dot{V}_{out}$ and yielded an output voltage, V_c, with $V_c = k_{p_a} V_{out} + k_{d_a} \dot{V}_{out}$. The aforementioned voltages across each capacitor were defined as

$$\Delta V_1 = V_b - V_c - \frac{V_x}{2} \qquad \Delta V_2 = V_b + V_c + \frac{V_x}{2}$$

with ΔV_1 and ΔV_2 representing the voltage across capacitor C_1 and C_2, respectively. Finally, combining the electrostatic forces, defined by $F_{el} = \frac{1}{2} C \Delta V^2$, for each capacitor in addition to the apparent forces of drag and thrust acting on the seismic mass culminates in the differential state equation for v_a,

$$\dot{v}_a = \frac{D - T}{m_{s/c}} + \frac{F_{el_1}}{m} - \frac{F_{el_2}}{m} \tag{4}$$

where $m_{s/c}$ and m denote the mass of GOCE and the seismic mass, respectively. Subsequently, the differential state vector for x_a is simply given with $\dot{x_a} = v_a$.

3.2 Solenoid Flow Control Valve

The solenoid flow control valve states are the position and velocity of the solenoid piston denoted x_v and v_v, respectively, and the current going into the solenoid coil, I. As aforementioned in Section 2.2, the piston is modelled as a point mass with a spring-dashpot and an additional force provided by the solenoid coil and thus, the differential state for v_v is given by

$$\dot{v}_v = \frac{1}{m_v} \left(K_v (x_0 - x_v) - K_i I - c v_v \right) \tag{5}$$

where m_v, x_0, K_i, and K_v signify the mass of the piston, the initial closed position, the current-force coefficient, and the spring constant, respectively. In addition, the differential state equation for x_v is simply $\dot{x}_v = v_v$. However, the differential state equation for I requires the V_{out} and $\dot{V}_{out}$ variables and is given by

$$\dot{I} = k_{p_v} \dot{V}_{out} + k_{i_v} V_{out} \tag{6}$$

and thus, the evaluation can be found alongside the determination of the differential accelerometer state equations within the implementation.

The position of the solenoid piston defines the opened area for the valve. The algebraic equations to define this open area, A_{op}, shown as section A-A in Figure 3, are given by

$$\alpha = 2 \left(\pi - \arccos \left(\frac{r_0 - x_a}{r_0} \right) \right) \qquad A_{op} = \frac{r_0^2}{2} (\alpha - \sin \alpha) \tag{7}$$

where r_0 is the radius of the valve. Following this, the mass flow rate, $\dot{m}$, passing through the valve can be determined, assuming choked flow, with,

$$\dot{m} = \frac{A_{op} P}{\sqrt{T}} \sqrt{\frac{\gamma}{R}} \left(\frac{\gamma + 1}{2} \right)^{\frac{\gamma+1}{2(\gamma-1)}} \tag{8}$$

where P, T, R, and γ denote the pressure, temperature, gas constant, and adiabatic ratio of the Xenon gas within the tank, respectively. The ion thruster utilises this mass flow rate to generate a thrust. Following the assumptions stated in Section 2.3, the overall thrust, T, generated by the ion thruster can be shown as,

$$T = \dot{m} \sqrt{\frac{2 e V_{grid}}{\mu}} \tag{9}$$

with e, μ, and V_{grid} being the charge and mass of the Xenon ions, respectively, and the voltage of the acceleration grid.

3.3 Keplerian Planetary Equations

In addition to the states for the accelerometer and the solenoid flow control valve, the keplerian elements are also present within the state vector as this is an orbiting spacecraft and the drag experienced must be simulated. The differential state equations for each of the keplerian elements can be seen in Equations 10 - 15. The perturbations for the keplerian elements are solely composed of the J_2 effect and the force of drag acting on the spacecraft due to the thermosphere and modelled accordingly with the DTM2013 atmosphere model and the standard J_2 perturbation equations in the RSW frame.[Cur13][ATM][Bru+][Bru15]

$$\begin{cases} \dot{h} = r p_s & (10) \\ \dot{e} = \dfrac{h}{\mu}\sin(\theta)p_r + \dfrac{1}{\mu h}\left[(h^2+\mu r)cos(\theta)+\mu e r\right]p_s & (11) \\ \dot{i} = \dfrac{r}{h}\cos(\omega+\theta)p_w & (12) \\ \dot{\Omega} = \dfrac{r}{h\sin(i)}\sin(\omega+\theta)p_w & (13) \\ \dot{\omega} = -\dfrac{1}{eh}\left[\dfrac{h^2}{\mu}\cos(\theta)p_r - \left(r+\dfrac{h^2}{\mu}\right)\sin(\theta)p_s\right] - \dfrac{r\sin(\omega+\theta)}{h\tan(i)}p_w & (14) \\ \dot{\theta} = \dfrac{h}{r^2} + \dfrac{1}{eh}\left[\dfrac{h^2}{\mu}\cos(\theta)p_r - (r+\dfrac{h^2}{\mu})\sin(\theta)p_s\right] & (15) \\ & (16) \end{cases}$$

Finally, the altitude calculation was performed by first assuming the Earth is an ellipse, as the spacecraft is in a pure polar orbit, and such, can follow the equation for the radius of an ellipse at a specific angle using the semi-major and semi-minor axis of earth and the latitude of the spacecraft.

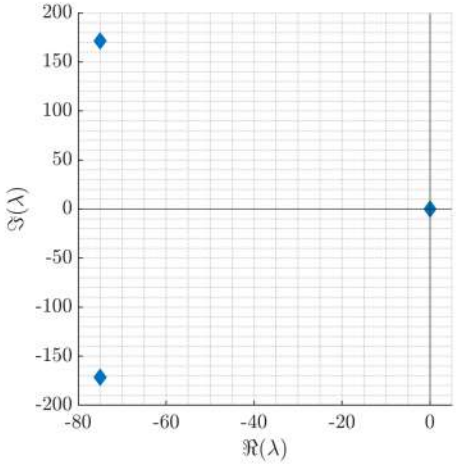

Figure 5: Eigenvalues found during linearisation of the complete system

In order to determine the most suitable numerical integration method for the proposed mathematical model an analysis of the corresponding eigenvalues was conducted. The model was decomposed into states and their complementing differential equations using Matlab's *symbolic toolbox*. Algebraic equations present within equations were substituted as variables to simplify the computation of the Jacobian matrix. The reference condition chosen for the linearisation coincides with a time shortly after the initial conditions, integrated with the commonly chosen `ode45` integrator, to avoid undefined calculations during the evaluation of the Jacobian and the corresponding eigenvalues can be seen in Figure 5. The majority of the eigenvalues are positioned at or near the origin with two positioned well within the left hand plane clearly suggesting that the model is a *stiff* system and thus, an appropriate integrator to accommodate stiff systems must be selected.

4 Numerical Integration

The variable order ODE integrator `ode15s`, an in-built Matlab integrator function capable of accommodating stiff systems, was adopted for the task. `ode15s` by default uses a Numerical Differential Formula (NDF) nonetheless, the optional Backward Differential Formula (BDF) was chosen for all integration runs. An alternative to the `ode15s` integrator is

`ode23s`. However, it was not selected due its ability of only varying up to the 3rd order, instead of the 5th, as with `ode15s`. Performing the integration of the system with a review of the order that has been used at certain time-steps shows, that the 4th and 5th order are exploited for the evaluation of given time steps. This fact indicates, that the `ode15s` integrator is the better choice for the derived model and `ode23t` and `code23tb` not even considered. The stability region of the `ode15s` integrator with the optional BDF method is shown in Figure 6, with all five orders presented. The lines enclose the numerically *unstable* regions, where the outer lines represent the higher orders. For the purpose of establishing the necessity, if needed, to enforce a tolerance within the integration, a numerical trade-off was also conducted. This trade-off was carried out by integrating the system over three orbital periods for several times in an attempt to mitigate the effects of Matlab's *Just-In-Time* compiler affecting the integration times, resulting in *coarse* and *fine* data. The *fine* data corresponds to tolerance enforcement and *coarse* data to no enforcement. As the final and main outcome of the system is the compensation of drag using thrust, the thrust was utilised as the benchmark. The resulting relative percentage difference between *coarse* and *fine* thrust suggests the tolerance enforcement is required when accurate data is desired however, when comparing general trends the integrator can be run without tolerance enforcement as the general error is approximately 1% and with no enforcement the integration is sped up by up to 40 times. The step-size of the integrator was also not fixed. This decision was based on performing another integration run and extracting the time-steps. The results showed that the range of time-steps lies over several orders of magnitude, which in turn states that to capture the physics accurately, the chosen time-step would be required to be the smallest, thus requiring a longer time period for the calculation to finish.

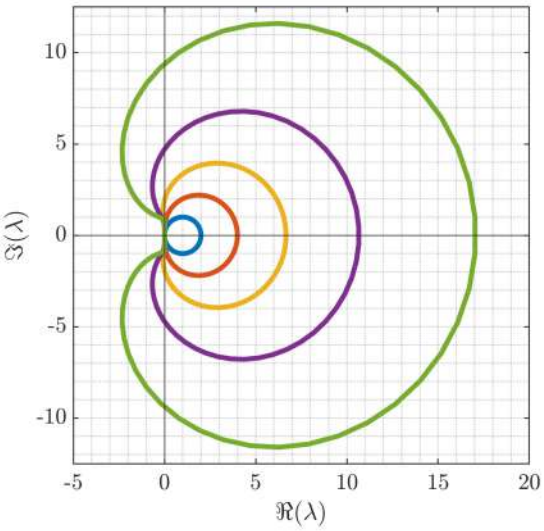

Figure 6: Stability regions of the BDF integrator

5 The simulation framework

The overall framework for the DFAC is represented as a flow diagram in Figure 7. Several helper functions were created to compartmentalise the problem into separate smaller functions, implementing the equations described in Section 3. This is done to calculate each individual component separately. All functions require the main `spacecraft` structure, which holds all the parameters required for the model with only a couple functions requiring the `planet` structure, a container for the data regarding the Earth. The order of the function calls depend on the values are required for each function. As an example, the `Accelerometer` requires both, the calculated drag and thrust, whereas the `Keplerian` function only

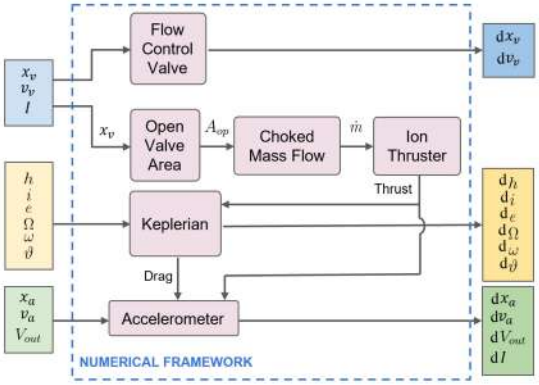

Figure 7: Flow chart depicting the structure and data flow of the main DFAC function. States are visible and arrows illustrate the flow of data. Functions are shown in pink and the names coincide with the created functions. If a variable is not specified on the arrow then all state variables are carried through.

requires the thrust, as this is where drag is determined. Furthermore, the thrust calculation demands only the state variables and hence corresponds to the first blocks within the flow.

6 System response

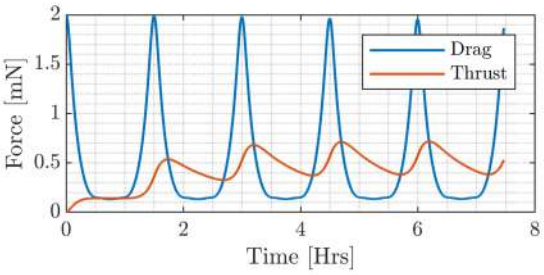

Figure 8: Distribution of drag with the determined counteracting thrust over five orbits at nominal conditions

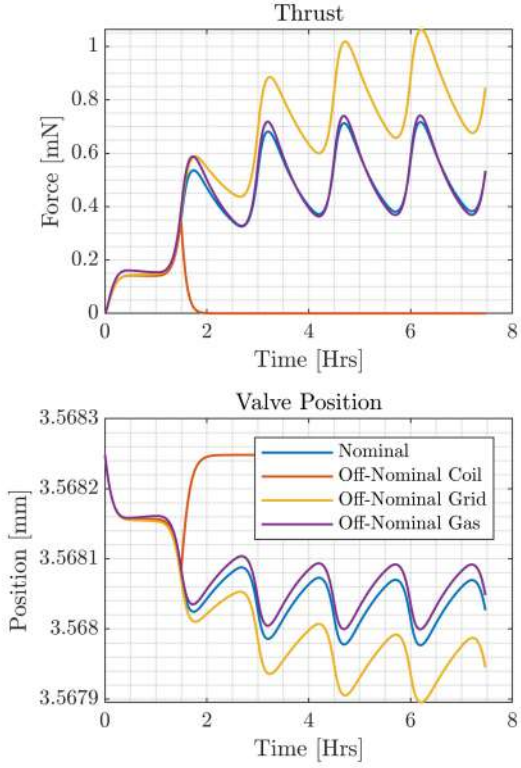

Figure 9: Comparison of nominal and off-nominal conditions for the thrust and the valve position

An integration run with nominal conditions has been executed over a time span of 5 orbital periods. The initial conditions of the system were chosen from its complete equilibrium. The position of the control valve piston is fully closed with its velocity equalling to zero. Furthermore, the seismic mass is initially at the reference point between the two electrodes, and all currents and voltages also at zero. The spacecraft is orbiting the Earth at an altitude of 254.9km, with an inclination of 90°, and an eccentricity of 0.0045. The results of the thrust response in comparison to the simulated drag is shown in Figure 8. From this figure it is clear that the current system parameter values do not achieve the desired drag-free result the scientific instruments desire and thus, needs to be optimised.

Additionally, three off-nominal cases were individually considered: the solenoid losing the ability to produce an effective magnetic force due to electrical failure, a long term power supply failure for the acceleration grid leading to a reduction in voltage over time, and a thermal design issue leading to a lower working temperature for the Xenon gas. The response for each off-nominal condition is presented in Figure 9, in comparison to the nominal condition for thrust and the flow valve piston position.

The solenoid failure mode occurs after one orbital period and decreases exponentially, in attempt to represent the solenoid dissipating stored magnetic energy. The valve position response can be seen to follow this exponential decay, resulting to a closed valve and null thrust.

The acceleration grid failure occurs at the start of the integration run and also decreases exponentially during the entire integration process, reaching a value of 100V at approximately hour 7. The decrease of the acceleration voltage and hence the thrust, causes a compensation through the control system takes place, decreasing the position of the piston and thus, opening the valve more. However, due to the slow responsiveness of the current system parameters this condition culminates in a higher overall thrust profile compared to the nominal case.

Finally, comparing the nominal and off-nominal case, in the event of the working temperature of Xenon, attaining a lower value than expected, shows similar responses. This suggests, that changes of gas temperature of up to 100K difference have only little affect on the overall performance and thus, is undeterred by non-optimal system parameters.

The most uncertain parameters of a model are those which are typically *tuned* when de-

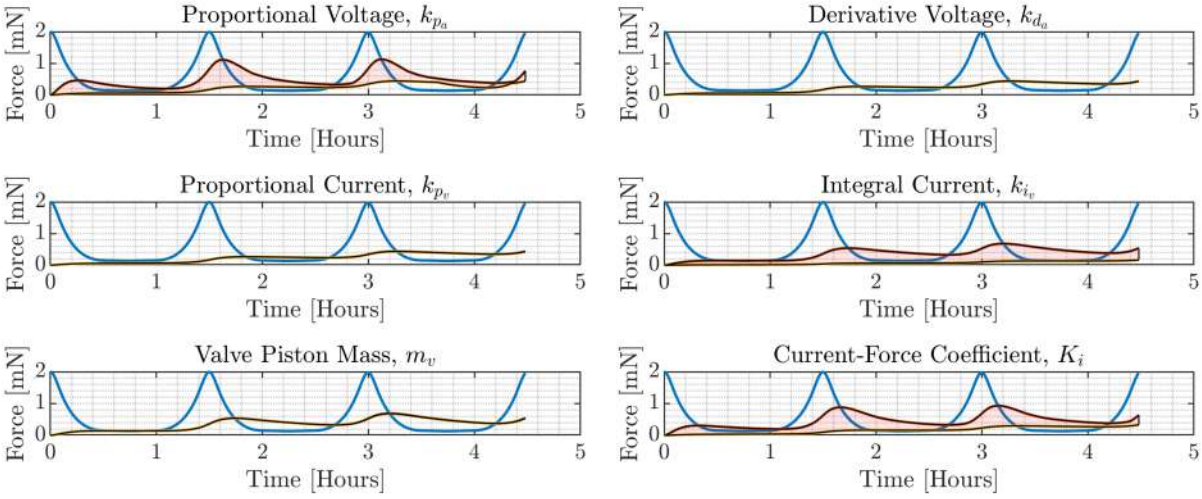

Figure 10: Sensitivity analysis of the most uncertain parameters being varied and their response envelope shown. Drag is shown in blue. The uncertain thrust response is shown as shaded red.

signing a system. The coefficients of the controllers in the accelerometer and the flow control valve, and both the solenoid valve piston mass, as well as the current-force coefficient have been chosen as the parameters to vary to further study their effect on the overall system response. This study consisted of varying each parameter ±83% from the corresponding nominal value and performing an integration run for each value. Each run was done over a predefined time span and time interval in order to extract the thrust values at a particular time step. The maximum and minimum at every time step was found in order to generate an upper and lower bounding line for each parameter. The area between this bounding lines was filled to highlight the uncertain response area created from varying an individual parameter. The results of this study can be seen within Figure 10, which clarifies that modifying the values for proportional coefficient of the voltage, integral coefficient of the current, and current-force coefficient of the solenoid value show a substantial effect, when modifying them.

7 System optimisation

As identified within Section 6 the current system parameters struggle to compensate the drag therefore, an optimisation is required. The parameters that, when varied, provided a noticeable effect on the thrust were selected as the optimisation variables. As the purpose of the control system is to provide a drag free environment the cost function will simple be the sum of the absolute differences between the thrust and drag at fixed intervals. In an attempt to speed up the optimisation process the optimisation variables were normalised and before performing the integration run multiplied by an exponent. The in-built Matlab function, `fmincon`, was adopted for this task.

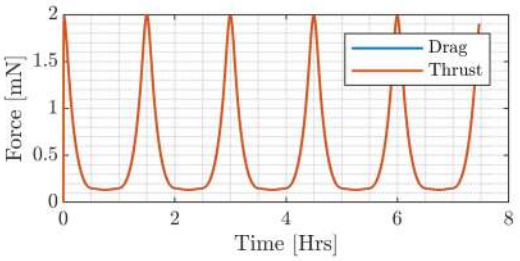

Figure 11: System response of the thrust against drag. The thrust with optimal parameters is able to compensate the drag.

The optimisation process was conducted enforcing no tolerances during the integration run to speed up the time taken per iteration and a local minima was found with the optimal thrust response shown in Figure 11. The optimal parameter values for k_{p_a}, k_{i_v}, and K_i are 1,970,110, 230.50, and 1.73, respectively. It is self-evident that the optimal values ensure the overall thrust response follows the drag closely, thus providing the coveted drag-free environment.

References

[13] *GOCE completes its mission.* 2013. URL: http://www.esa.int/Applications/Observing_the_Earth/GOCE/GOCE_completes_its_mission.

[ATM] ATMOP. *Advanced Thermosphere Model for Orbital Prediction.* URL: http://atmop.eu/.

[Bru+] Sean Bruinsma and CNES-Space Geodesy. *Thermosphere model evaluation at low altitude with GOCE densities.*

[Bru15] Sean Bruinsma. "The DTM-2013 thermosphere model". In: *Journal of Space Weather and Space Climate* 5 (Feb. 2015). DOI: 10.1051/swsc/2015001.

[Can+09] Enrico Canuto and Luca Massotti. "All-propulsion design of the drag-free and attitude control of the European satellite GOCE". In: *Acta Astronautica* 64.2 (Jan. 2009), pp. 325–344. DOI: 10.1016/j.actaastro.2008.07.017.

[Cur13] Howard D Curtis. *Orbital mechanics for engineering students.* Butterworth-Heinemann, 2013.

[Edw+] CH Edwards et al. "The T5 ion propulsion assembly for drag compensation on GOCE". In:

[Gin+14] Francesco Gini et al. "Precise orbit determination for the GOCE re-entry phase". In: *Proceedings of the fifth international GOCE user workshop.* 2014.

[Kli16] Sergei A Klioner. "Basic Celestial Mechanics". In: *arXiv preprint arXiv:1609.00915* (2016).

[Len+11] Benjamin Lenoir et al. "Electrostatic accelerometer with bias rejection for gravitation and Solar System physics". In: *Advances in Space Research* 48.7 (Oct. 2011), pp. 1248–1257. ISSN: 0273-1177. DOI: 10.1016/j.asr.2011.06.005. URL: http://dx.doi.org/10.1016/j.asr.2011.06.005.

[Mar+03] P. Martella et al. "The GOCE Drag Free and Attitude Control Design Aspects and Expected Performance". In: *Spacecraft Guidance, Navigation and Control Systems.* Ed. by K. Fletcher and R. A. Harris. Vol. 516. ESA Special Publication. Feb. 2003, p. 331.

[Nic+18] Luca Nicolini and Alessandro Caporali. "Investigation on Reference Frames and Time Systems in Multi-GNSS". In: *Remote Sensing* 10.2 (2018), p. 80. DOI: 10.3390/rs10010080.

[Tou+99] P Touboul et al. "Accelerometers for CHAMP, GRACE and GOCE space missions: synergy and evolution". In: (1999).